Published in final edited form as:

Dev Cell. 2016 January 11; 36(1): 24–35. doi:10.1016/j.devcel.2015.12.013.

Emergence of an apical epithelial cell surface *in vivo*

Jakub Sedzinski[1,*], **Edouard Hannezo**[2,3,*], **Fan Tu**[1], **Maté Biro**[4,5], and **John B. Wallingford**[1,6,**]

[1]Dept. of Molecular Biosciences, Center for Systems and Synthetic Biology, and Institute for Cellular and Molecular Biology, University of Texas at Austin, Austin, TX 78712, USA.

[2]Cavendish Laboratory, Department of Physics, J.J. Thomson Avenue, University of Cambridge, Cambridge CB3 0HE, UK

[3]Wellcome Trust/Cancer Research UK Gurdon Institute, University of Cambridge, Tennis Court Road, Cambridge CB2 1QN, UK

[4]Centenary Institute of Cancer Medicine and Cell Biology, Locked Bag 6, Newtown, NSW 2042, Australia

[5]Sydney Medical School, The University of Sydney, Sydney, NSW 2006, Australia

[6]Howard Hughes Medical Institute

Abstract

Epithelial sheets are crucial components of all metazoan animals, enclosing organs and protecting the animal from its environment. Epithelial homeostasis poses unique challenges, as addition of new cells and loss of old cells must be achieved without disrupting the fluid-tight barrier and apicobasal polarity of the epithelium. Several studies have identified cell biological mechanisms underlying extrusion of cells from epithelia, but far less is known of the converse mechanism by which new cells are added. Here, we combine molecular, pharmacological and laser-dissection experiments with theoretical modelling to characterize forces driving emergence of an apical surface as single nascent cells are added to a vertebrate epithelium *in vivo*. We find that this process involves the interplay between cell-autonomous actin-generated pushing forces in the emerging cell and mechanical properties of neighboring cells. Our findings define the forces driving this cell behavior, contributing to a more comprehensive understanding of epithelial homeostasis.

**Corresponding author: Patterson Labs, University of Texas, 2401 Speedway, Austin, TX 78712, USA. Wallingford@austin.utexas.edu, 512-232-2784.

*These authors contributed equally to this work.

***Author* Contributions:**

J.S., E.H., and J.B.W. designed the research and wrote the paper; J.S. performed the experiments; M.B. developed the image analysis tools; J.S., E.H. analyzed the data; F.T. contributed to experimental procedures; E.H. developed the theoretical model.

Introduction

Development and homeostasis of epithelial sheets depends upon the regular addition of new cells and removal of old cells (Macara et al., 2014). In some cases, new cells are added by divisions within the cell sheet, but in other cases new epithelial cells are derived from a distinct population of basally-located progenitors. Indeed, such basal stem cells have been described in the airway, olfactory epithelium, cornea, and prostate, among others (Cotsarelis et al., 1989; Evans and Moller, 1991; Ford and Terzaghi-Howe, 1992; Leung et al., 2007; Rock et al., 2009; Tsujimura et al., 2002). In such multi-layered tissues, newly born epithelial cells join the existing epithelial sheet by a series of coordinated cell behaviors collectively known as radial intercalation (Fig. S1A). Radial intercalation is a complex process which, at a minimum, requires the nascent cell to 1) define an apical-basal axis and assign apical identity; 2) move apically and separate the basolateral surfaces of overlying cells in the epithelium; 3) make contact with the lumen by penetrating the tight junctions of the epithelium; 4) remodel those junctions in order to maintain barrier function; 5) build an apical surface of sufficient size to accommodate the new cells function (e.g. directional beating in a ciliated cell; luminal secretion in a secretory cell, etc.).

This final process of apical surface “emergence” (Figure 1A; Supp. Figure S1A) is of particular interest and can be envisioned perhaps most simply as the converse of apical constriction, a well-defined cell behavior underlying both epithelial cell extrusion and epithelial folding (Guillot and Lecuit, 2013; Martin and Goldstein, 2014). While both molecular and mechanical aspects of apical constriction have been extensively studied, almost nothing is known of apical emergence.

One important example of radial intercalation is provided by multiciliated cells (MCCs) in mucociliary epithelia (Brooks and Wallingford, 2014). In both the mammalian airway and in the well-studied model system of the *Xenopus* epidermis, MCCs arise from basally located p63+ progenitor cells (Supp. Figure 1A; (Evans et al., 2001; Lu et al., 2001; Rock et al., 2009; Stubbs et al., 2006). The cell biological mechanisms controlling radial intercalation in airway MCCs remains to be explored, but there have been substantial advances recently in understanding this process in *Xenopus*. For example, we showed that the transcription factor Rfx2 was essential (Chung et al., 2014), and others have shown roles for Laminin/Dystroglycan, Rab11, and the Par complex (Kim et al., 2012; Sirour et al., 2011; Werner et al., 2014). These latter findings are significant because apical emergence during radial intercalation resembles in many respects *en masse* apical surface formation during lumen morphogenesis in tubular organs, a process that also involves Laminin, Rab11, and the Par complex (Datta et al., 2011).

A major outstanding question regarding radial intercalation of MCCs concerns force generation during apical emergence. Force generation within cells and force transduction between cells are exquisitely regulated during cell movement (Guillot and Lecuit, 2013; Heisenberg and Bellaiche, 2013; Mao and Baum, 2015; Ng et al., 2014). We therefore sought to understand the physical mechanisms that drive the growing apical surface as a new cell emerges in the epithelium and also those forces that displace the emerging cell’s neighbors. These questions are important because the answers will provide an essential

complement to the burst of recent studies elucidating mechanisms of force generation during extrusion of old cells from epithelia (e.g. (Eisenhoffer et al., 2012; Marinari et al., 2012; Wu et al., 2014). Here, we address this issue, using *in vivo* imaging, quantitative modelling, laser microdissection, and molecular manipulations to show that apical emergence in nascent MCCs is a predominantly cell-autonomous process driven by Formin1-dependent actin-based pushing.

Results

Apical emergence is driven cell autonomously in the apical region of nascent MCCs

Exploiting their large size and experimental tractability (Werner and Mitchell, 2011), we examined apical emergence in *Xenopus* MCCs using a transgenically-expressed actin biosensor and membrane-targeted fluorescent proteins. Three-dimensional time-lapse imaging revealed that MCC apical cell surface emergence was highly stereotyped from cell to cell, with apical area increasing in a consistently sigmoidal pattern (Figures 1B–D; Movie S1). Perhaps the simplest mechanism that might drive emergence would involve cell-autonomous actomyosin contraction of the basal cell surface exerting pressure on the incompressible cytoplasm and thereby forcing expansion of the apical surface (Figure 1E, pink arrows). Indeed, such basal constrictions have been reported during epithelial morphogenesis (e.g. (Gutzman et al., 2008). A second, related model that might explain apical emergence involves an apicobasally-directed actomyosin contraction acting to decrease cell height (e.g. (Sherrard et al., 2010); like basal constriction, this type of force could collaborate with incompressible cytoplasm to expand the apical surface (e.g. Figure 1E, purple arrows). However, several lines of evidence from our 4D imaging argue against these two models.

First, quantification of cell shapes during emergence showed no evidence for basal constriction of cells or of apicobasal cell shortening (Figures 1F and 1G). MCC emergence was accompanied by little or no shape change in the medial or basal regions of the cell (Figures 1F and S1B; Movie S2). Moreover, we observed an increase in cell volume during the process, which would limit the ability of basal constriction or apicobasal shortening to exert pressure on the apical surface (Figures 1G and S1C). Most importantly, using trangenic expression of actin and myosin reporters specifically in MCCs, we observed no accumulation in basolateral regions (Figures 1C, S1B, S1C and S2A), in contrast to what has been observed in known instances of basal constriction and cell shortening (Gutzman et al., 2008; Sherrard et al., 2010). In fact, as described in detail below, we observed just the opposite: apical emergence was strongly correlated with enrichment of apical actin in nascent MCCs.

Another plausible model can be envisioned whereby apical emergence is driven by a 2D pulling force parallel to the apical surface that is exerted by apical constriction in cells abutting the nascent MCC (Figure 1E, blue arrows). We tested this model in two ways. First, if actomyosin contraction of neighbouring cells pulled upon emerging MCCs, we might expect that the increasing apical surface area of emerging MCCs would negatively correlate with the apical area of the neighboring cells. However, this trend was never observed. Rather, the apical area of neighboring cells actually increased modestly during MCC

emergence (Figures 2A and 2F; Figures S3A–C), likely due to changing global tensions exerted on this epithelium by the developing embryo.

As a more direct test of this neighbor-pulling model, we reasoned that if neighboring cells were exerting tension on the MCC and thereby effecting emergence, then tension release of neighboring cells should result in a rapid collapse of the MCC apical cell surface. We tested this idea using laser ablation of neighboring cells (Figures 2C and 2E top). We saw no dramatic changes in the apical area of MCCs upon adjacent cell ablation (blue/red traces in Figures 2F and 2G). This was true regardless of whether ablation was targeted to the center of the neighboring cell or to its cell-cell junctions (Figure S3D,E).

As an additional test of neighboring-pulling model, we used transverse (X–Z) optical sections to quantify the shape of the interfaces joining MCCs to neighbors as they were ablated (X/Z view in Figures 2B, 2D and 2E bottom). Strikingly, laser ablation of the neighbor led to its collapse and clearly resulted in tension being exerted on the MCC, as evidenced by the change in shape of the interface between the MCC and the ablated cell (φ_1 in Figure 2E; black trace in Figure 2G).. No such change was observed on the opposite side of the MCC (φ_2 in Figure 2E; green trace in Figure 2G). Importantly, despite the tension imparted to the MCC (apparent from the change in φ_1), the MCC apical surface area was not substantially altered (red trace in Figure 2G). Together with the experiments arguing against cell autonomous basal constriction or apicobasal shortening, these findings argue that apical emergence is accomplished via action within the emerging apical domain of the MCC itself.

Theory and experiment suggest that MCC apical emergence is driven cell-autonomously by an effective 2D pressure in the apical cell surface

Cell motile behaviors emerge *in vivo* from a complex tug-of-war influenced by the mechanical properties of both the moving cell and its neighbors (Guillot and Lecuit, 2013; Heisenberg and Bellaiche, 2013; Mao and Baum, 2015). Because our experiments ruled out three simple models that might explain apical emergence, we turned to quantitative modelling to gain new insights into this cell behavior. We developed a minimal theoretical model in which we assume that apical surface area is the product of the force balance exerted on an apical cell membrane by intrinsic and extrinsic forces (Figure 3A; see Supplemental File S1, Theory). Because apical emergence in *Xenopus* MCCs is slow (hours) (Chung et al., 2014; Stubbs et al., 2006), we assume that viscosity plays a negligible role, and that the dynamics of the expansion are dictated by the time it takes to build up the driving force. We write the force balance on the apical surface of the MCC, in polar coordinates, for an MCC apical radius r as a function of angle θ:

$$0 = -\gamma K + \delta P - Er + \Lambda \sum_i \delta(\theta - \theta_i) \quad (1)$$

Where K is the local curvature, Λ and γ are junctional line tensions from the perpendicular junctions of the neighbors and the intercalating cell, respectively; E is a resistance from the surrounding cells, and δP is an effective 2D pressure generated at the apical domain of the emerging MCC (Figure 3A). In this model, apical expansion is resisted both by the rigidity of the neighboring cells and by the expanding cell's own cortex. Conversely, two forces could potentially drive expansion: the effective 2D pressure in the expanding cell (intrinsic

pushing forces; Figure 3A, black arrows) or the tension of the perpendicular junctions along neighboring cells (extrinsic pulling forces; Figure 3A, red arrows). We note that this model restricts itself to force generation in two dimensions, which is consistent both with theoretical considerations (Supplemental File S1, Theory, section 1.5) and with our findings above (Figure 1 and Figure 2).

The two potential driving forces in this model are expected to generate very different cellular shapes during emergence, depending upon which force is dominant (Supplemental File S1, Theory, section 1.2). When pushing forces in the MCC (δP) are dominant, the model generates round-shaped cells (Figure 3B). When pulling forces from perpendicular junctions between neighboring cells are dominant, the model generates polygonal-shaped cells with well-defined angles (Figure 3C). To ask which of these two possibilities better reflected the *in vivo* situation, we quantified apical surface shapes from time-lapse movies of emerging MCCs. Using an angularity parameter which equals zero if the cell is round and increases for more polygonal shapes (Kurtosis; Supplemental File S1, Theory, section 1.3), we systematically observed that MCCs remained rounded during the bulk of their emergence, and transitioned from round to polygonal only at the end of this process (Figure 3D; Movie S1). This trend was highly stereotyped from cell to cell (Figures 3E and 3F). We then challenged this correlation with an experimental test by quantifying the tension in neighboring cells' junctions using laser microdissection, in which initial recoil velocities after cutting provide an effective proxy for cell junctional tension. We severed neighboring cell junctions that were perpendicular to MCCs (Figure 3G; Λ in our model), finding that tension in these neighboring junctions remained low during the bulk of emergence and increased near the end of the process (Figure 3H). This result is in agreement with our angularity measurements (Figure3E and 3F) and suggests that intrinsic pressure is the main driver of the bulk of MCC apical emergence and that line tension from neighboring cell cortices only contributes to refinement of apical domain shape at the later stages.

Next, we performed numerical simulations of Eq. 1, fitting the time evolution of the angularity and apical radius to extract the parameters (Supplemental File S1, Theory, Section 1.4). Our model accurately reproduced the apical surface shape changes throughout MCC emergence, from round to polygonal (Figures 3I and S4) and allowed us to infer the time evolution of junctional tension, Λ and an effective 2D pressure, δP (Figures 3J and 3K). Altering the various parameters gave rise to a variety of clearly distinguishable shapes, strengthening our fit (Supplemental File S1, Theory, Section 1.4). This theoretical analysis yields three main predictions: 1) That the temporal pattern of neighboring junctional tensions will mirror the angularity parameter; 2) That a slowly increasing 2D pressure drives emergence; and 3) That emergence is driven cell-autonomously, with surrounding cells resisting this process.

Assembly of the MCC apical actin network correlates closely with apical emergence

Both our cell shape and laser ablation data argued against pulling by neighboring cells, while imaging experiments argued against basolateral actomyosin contraction within the MCCs. Conversely, our quantitative model suggested that emergence could be driven cell autonomously by an effective 2D pressure within the apical surface of emerging MCCs (δP

in our model). While mechanisms by which such pressure may be exerted are unknown, MCCs are characterized by a complex apical actin network that is essential for the normal polarization and motility of the cilia decorating the apical surface of MCCs (Pan et al., 2007; Werner et al., 2011). However, we observed that the initial assembly of this meshwork coincident with MCC apical surface emergence (Figures 1B and 3D). Interestingly, actin is capable of generating significant pushing force, both *in vitro* and *in vivo*, for instance during lamellipodial extension (Demoulin et al., 2014; Kovar and Pollard, 2004; Mogilner and Oster, 2003; Prass et al., 2006; Yang et al., 2007). We reasoned, therefore, that the apical actin meshwork could be the source of the effective apical 2D pressure driving MCC emergence.

To test this idea, we quantified apical actin in MCCs, normalizing among different samples and experiments using the ratio of medial to junctional actin (Figures 4A, 4B; Movie S3). We found a robust positive linear correlation between increasing apical area and apical actin concentration (Figures 4C and 4D). Moreover, the slope of this curve was highly conserved, such that we could collapse all cells on the same master curve (Figure 4E). By contrast, a similar analysis of apical Myosin II revealed no correlation (Fig. S2C). In addition, we assessed the relationship between cell-cell adhesion and apical emergence using E-Cadherin-GFP expressed specifically in MCCs. Strikingly, we observed no correlation between cortical E-Cadherin levels and the change in MCC apical area (Fig. S2B, D). These data contrast with the strong correlation we observed between medial actin assembly and apical area and thus suggest that remodelling of cellular adhesions does not produce force for emergence. This result is consistent with recent reports from zebrafish and *Drosophila*, arguing that cadherins are not generally involved in force generation during morphogenesis, but rather integrate and transmit forces generated by the cytoskeleton (Collinet et al., 2015; Maitre et al., 2012; Rauzi et al., 2010). Overall, these results are consistent with a model wherein apical actin network assembly generates the 2D pressure suggested both by our model and by our laser-cutting data.

Formin1 essential for apical emergence

In order to explore the hypothesis that actin network assembly generates the 2D pressure for apical emergence, we must first appreciate the mechanical relationships between 2D pressure (δP) and cell junctional tension (γ) in MCCs (Fig. 3A). Theoretically, the existence of a junctional tension γ should result in a critical radius $r_c \approx \frac{\gamma}{\delta P}$, below which the pressure forces cannot balance the tension. For a given pressure, if the cell radius is below this critical value, a collapse is expected. The simplest, first order assumption taking this into account is to write junctional tension as linearly increasing with MCC radius:

$$\tau \partial_t \gamma = -\gamma + \gamma_0 r$$

where τ is the response time between changes in radius and tension, and γ_0 the target tension at steady state (i.e. for a rescaled final radius r = 1).

Using this model, we can assemble a phase diagram of potential emergence behaviors, as a function of the target tension γ_0 and pressure δP, for a given time delay. With high δP

pressures, apical area undergoes a monotonic sigmoidal increase, as observed in both our simulations and in normal cells *in vivo* (Figure 5A, expansion). However, when pressures are low, the tension builds up too quickly, the cell radius becomes smaller than the critical threshold, and the apical surface collapses (Figure 5A, collapse). For intermediary pressures, a third cell behaviour appears, where the apical area overshoots its steady state value, then undergoes damped oscillations. This occurs because of the delay time for the tension to build-up, which allows an apical area to grow excessively before tension catches up and reduces it (Figures 5A, overshooting, 5D; Movie S4).

To test this aspect of our model experimentally, we needed first to identify a mechanism by which to modulate 2D pressure in MCCs. Because we predict that this pressure is generated by apical actin network assembly (Fig. 4), we took advantage of our previous finding that the Rfx2 transcription factor is essential for MCC emergence (Chung et al., 2014). Among the direct targets of Rfx2, we found Formin 1 (Fmn1), and formins regulate actin assembly and actin-based pushing (Block et al., 2012; Kobielak et al., 2004; Yang et al., 2007). Consistent with a possible role for this protein in emergence, we found that Fmn1-GFP was enriched apically in MCCs (Figure S5A).

Noting that both our modelling and laser ablation data suggest that apical emergence is driven cell-autonomously, we tested the cell-autonomous requirement for Fmn1 action using mosaic knockdown (see experimental procedures). MCCs lacking Fmn1 function frequently exhibited catastrophic collapse of the emerging apical cell surface (Figures 5B, 5E blue line and S5B; Movie S5), a behavior our model predicts should result from specific reduction of the apical 2D pressure (δP) (Figure 5A). As a control for the knockdowns, we also found that similar apical collapse resulted from MCC-specific expression of dominant-negative Fmn1 (DN-Fmn1; Figure S5C). By contrast, disruption of Fmn1 in neighboring cells, either by knockdown or by expression of DN-Fmn1 never elicited MCC apical collapse (Figures 5C and 5E black line).

Interestingly, not all cells exhibited a collapse behaviour after manipulation of Fmn1 function. Some cells displayed the “overshoot” behaviour predicted in our model (Figures 5D and 5F), and others displayed simply a reduced overall rate of apical surface emergence (Figure 5G; Supplementary Table 1). In light of this spectrum of phenotypes, we performed an additional test of the model, using a small molecule formin inhibitor to ask if acute disruption of Formin function also causes apical collapse. Consistent with our hypothesis, application of Smifh2 (Rizvi et al., 2009) elicited striking collapses of emerging MCC apical surfaces (Figure 5H). These data argue that Fmn1, a known regulator of actin dynamics is required cell autonomously for MCC apical emergence, consistent with our model in which apical actin network assembly generates the 2D pressure to drive MCC emergence.

Modulation of cell cortex tension in MCCs facilitates apical emergence

We next turned our attention to the interplay between the apical 2D pressure and the MCC’s own junctional tension (γ). Our theoretical model predicts that early during emergence, when the apical domain is small and 2D pressure (δP) is still low, collapse can occur as a consequence of high junctional tension within the MCC. This prediction raises the question of how 2D pressure in a normally emerging MCC overcomes the constricting force

generated by its own actomyosin cortex. One possibility is that in order to emerge, tension in the MCC cortex must initially decrease, thereby allowing expansion and preventing collapse. To test this prediction, we probed the junctional tension of MCCs by severing the cell junctional cortex by laser ablation (Figure 5I). Consistent with our model, we observed that at the onset of emergence, MCC junctional tension dropped from an initially high value (Figure 5J). During later stages, when pulling by neighboring cells begins to shape the MCC apical surface (Figure 3E, 3F and 3J), MCC junctional tension rises again (Figure 5J).

Neighboring epithelial cells mechanically resist MCC apical emergence

Our data suggest that emergence of the apical cell surface in MCCs is driven predominantly by an actin/formin-dependent 2D pressure within the MCC itself. However, any behavior of single cells within an intact epithelium will be impacted by the physical properties of the surrounding cells (Guillot and Lecuit, 2013; Heisenberg and Bellaiche, 2013; Mao and Baum, 2015). For example, extrusion of epithelial cells is known to involve a tight coordination between the cytoskeleton of the extruding cell and that of its neighbors (Marinari et al., 2012; Rosenblatt et al., 2001). Our theoretical model suggests a similar interplay, as Eq. 1 predicts that the MCC apical radius will be proportional to pressure and inversely proportional to neighbor rigidity ($r \approx \frac{\delta P}{E}$ in the limit of low tensions).

Since RhoA levels can tune cellular rigidity (Hannezo et al., 2014; Wakatsuki et al., 2003), we tested this prediction by transgenically expressing constitutively-active (CA) or dominant-negative (DN) RhoA specifically in neighboring cells and examining the effects on MCC emergence. Consistent with our model, excessive RhoA activity in neighboring cells resulted in slower MCC emergence and a smaller MCC apical size, while decreased RhoA activity in neighboring cells elicited the opposite result, larger apical cell surfaces compared to controls (Figures 6A–6D; Movie S6).

This experimental paradigm also provided an additional test of our model for actin-based 2D pressure. If our model of cell-autonomous emergence is correct, then we expect the area of MCCs to increase when neighboring cells are less rigid and to decrease when neighbors are more rigid. Consistent with this, DN-RhoA expressed in neighboring cells non-autonomously elicited an increase in apical area, for a given apical actin level in adjacent, un-manipulated MCCs (Figure 6E, blue). The converse was observed in MCCs with neighbors expressing CA-RhoA (Figure 6E, pink).

Finally, because the slope of the radius vs. pressure curve is equal to the inverse of the resistance 1/E (Supplemental File S1, Theory, Section 1.2), we can then extract this parameter for each condition, assuming as before that pressure is proportional to actin concentration. This leads us to CA-RhoA neighboring cells being 160% (+−20%) more rigid than wild type, and DN-RhoA neighboring cells being 50% (+−8%) more compliant than wild type (Figure 6E). Together, these data demonstrate that the rigidity of neighboring epithelial cells resists the autonomous, pressure-driven, apical expansion of MCCs, as predicted by our model.

Discussion

Here, we have begun to unravel the mechanical basis of a crucial but poorly understood cell biological process: emergence of the apical cell surface as an individual nascent cell radially intercalates into an existing epithelium *in vivo*. We have focused on multiciliated cells in the *Xenopus* epidermis, where studies over the last decade have sketched a molecular framework for the control of radial intercalation (Chung et al., 2014; Kim et al., 2012; Sirour et al., 2011; Werner et al., 2014). Our work adds Fmn1 to this framework and also provides the first glimpse of the mechanics at work here. Like *Xenopus* MCCs, those in the mammalian airway face the same challenges, as they are homeostatically replaced from basal stem cells (Evans and Moller, 1991; Ford and Terzaghi-Howe, 1992; Rock et al., 2009). Indeed, the principles uncovered here should inform our understanding of diverse epithelial cell types that are replenished from basally-positioned progenitor populations, for example in the cornea, olfactory epithelium, and prostate (e.g. (Cotsarelis et al., 1989; Leung et al., 2007; Tsujimura et al., 2002).

An interesting parallel to the apical emergence process studied here in individual cells is the *en masse* emergence of apical surfaces during lumen formation in tubular organs. Lumen formation is now well-defined, proceeding through a molecular hierarchy in which cell-cell or cell-matrix contacts provide cues for assembly of apicobasal polarization machinery, which in turn directs vesicle mediated delivery of new membrane to the growing apical surface (Datta et al., 2011). Key players in this process include laminin/integrin-based adhesion, polarity modules such as the Par3/aPKC complex and Crb3, and vesicle targeting small GTPases such Rab11 (Bryant et al., 2010; Yu et al., 2005). Strikingly, these very molecules are also implicated in radial intercalation in *Xenopus* MCCs (Kim et al., 2012; Sirour et al., 2011; Werner et al., 2014). By extension, it is possible that an actin-based pushing mechanism similar to that described here may also contribute to apical surface expansion during lumen formation. Indeed, coordination of the apical actin cytoskeleton is essential for lumen formation in both vertebrate and invertebrate tubular organs (Massarwa et al., 2009; Saotome et al., 2004). Conversely, there is also evidence that the apical emergence machinery may play cell-type specific functions, especially in MCCs. For example, Crb3 is central to apical determination, and has been shown to act via a known mechanotransducer to influence MCC cell fate in the airway (Szymaniak et al., 2015).

Another significant finding here is that actin-based pushing appears to drive apical emergence. Several lines of evidence support such a model: Imaging of cell shapes and actomyosin argue against cell-autonomous actomyosin-based models for emergence (Figures 1 and 2, Supp. Figures 1 and 2). Laser cutting likewise argues against actomyosin contraction of neighbors as a driving force for MCC emergence (Figure 2; Supp. Figure 3). By contrast, modelling, cell shape analysis, imaging of actin, and manipulations of Formin1 all argue that MCC emergence is driven largely by a cell autonomous, actin-based 2D pressure (Figures. 3, 4 and 5; Figures S4 and S5). While polymerization of both linear and branched actin has been shown to generate force to direct cellular process (e.g. (Demoulin et al., 2014; Kovar and Pollard, 2004; Mogilner and Oster, 2003; Prass et al., 2006)), the precise mechanism of actin pushing during emergence remains mysterious. Single actin filaments produce only very small forces, though bundled and/or cross-linked actin can

generate higher forces, so it is notable that Fmn1 is only one of many actin-regulators that are direct targets of Rfx2, a transcription factor essential for MCC apical emergence (Chung et al., 2014).

In addition to these insights into apical surface formation, our study of emergence of new cells also provides an important complement to studies of extrusion and delamination of old cells during epithelial homeostasis (Eisenhoffer et al., 2012; Marinari et al., 2012; Wu et al., 2014). Interestingly, extrusion is a cooperative process involving contractile forces of actomyosin systems in both the extruded cell and its neighbors (Marinari et al., 2012; Rosenblatt et al., 2001; Wu et al., 2014). Likewise, our data argue that MCC apical emergence also results from a delicate balance of different phases of cell-intrinsic, followed by cell-extrinsic forces. This balance is required for the optimal insertion and maturation of an apical surface, as the existence of junctional MCC tension creates a critical radius that cells have to pass in order to avoid collapse. Once this critical radius is passed, cell-extrinsic junctional forces increase in order to shape a mature epithelium.

Finally, just as actomyosin-based contractions drive cell extrusion in both normal homeostasis (Gibson and Perrimon, 2005; Marinari et al., 2012; Shen and Dahmann, 2005) and also pathologically during tumor dissemination (Wu et al., 2014), so too might the mechanisms of apical emergence described here be hijacked by cancer cells to drive invasion into epithelial tissues. Indeed, cancers in multi-layered epithelia are often characterized by differentiation defects that prevent suprabasal movement and lead to basal cell accumulation (e.g. (Driessens et al., 2012)). This process could bear similarities to the defective emergence observed here when Fmn1 function is disrupted. Thus, this study highlights the importance of understanding cell mechanics, not only in the context of morphogenesis, but also in tissue homeostasis and disease pathology.

Experimental Procedures

Xenopus embryo manipulations

Xenopus embryo manipulations and injections were carried out using standard protocols, see Supplemental Experimental Procedures for details.

Cloning, plasmids, morpholinos, and drugs treatment

For nectin driven expression of DNRhoA or CARhoA, the Open Reading Frame (ORF) of human DNRhoA or CARhoA was amplified by PCR from addgene.org provided plasmids (#15901 and #15900, respectively) and enzymatically subcloned into nectin driven expression plasmid containing RFP expression tag. α-tubulin GFP-UtrCH and a-tubulin RFP-UtrCH plasmids are described in (Chung et al., 2014). Nectin GFP-UtrCH or nectin RFP-UtrCH plasmids were generated by PCR reaction of nectin sequence and enzymatic substitution of α-tubulin promoter in aforementioned plasmids. FMN1 was amplified from standard *Xenopus laevis* cDNA prepared by reverse transcription (SuperScriptIII First strand synthesis, Invitrogen) via PCR amplification using following primers: FMN1_forward: CACCATGGAAGGCAAACACTCCAT, FMN1_reverse: GTTGCTGGTGACACTTG and then subcloned into gateway ENTRY clone (pENTR™/D-TOPO® Cloning Kit, Life

Technologies). GFP-FMN1 expression plasmid was made by LR reaction of entry-FMN1 clone and destination vector Pcsegfpdest (a gift from Lawson Lab), using Gateway® LR Clonase® II Enzyme mix (Life Technologies). Dominant negative version of FMN1 (DNFMN1) was constructed by cloning of PCR-generated region of the wild type FMN1 lacking FH1 and FH2 behind α-tubulin driven promoter using Gateway system.

Formins were inhibited with SMIFH2 (Rizvi et al., 2009)(Tocris Bioscience), by 45 min treatment at 50μM. Splice-blocking morpholino-oligonucleotides (MO) were designed and prepared by GeneTools. FMN1-MO sequence: 5'-(TCAGGCTGGATGATAGGAGACAAAA) -3'.

Morpholino oligonucleotide, mRNA, and plasmids injections

Capped mRNA was synthesized using mMessage mMachine kits (Ambion). Unless specified in the main text, mRNA, antisense MO or plasmids were injected into the two ventral blastomeres to target the MCCs epidermis. For mosaic injections of FMN1 MO, embryos at four-cell stage were injected into the two ventral blastomeres with α-tubulin GFP-UtrCH and subsequently injected with mixture of FMN1-MO and RFP-UtrCH mRNA (used here as an indicator of targeted FMN1-MO expression) into V11 and V12 blastomeres at sixteen-cell stage (Moody, 1987).

Live imaging of apical expansion

Embryos stage ~18–20 were mounted in 0.8% w/v Low Melting Point Agarose (LMPA), covered in 1/3 MMR and imaged at 23°C with a Zeiss LSM700 confocal microscope using C-Apochromat 40× 1.2 NA water immersion objective.

Immunostaining of whole embryos

Embryos injected with α-tubulin GFP-UtrCH into two ventral blastomers were fixed, immunostained, and cleared according to the protocol described in (Lee et al., 2008). Anti-GFP antibody (abcam, ab13970) dilution 1:500 was used to detect the GFP-UtrCH protein.

Laser ablations

Local laser ablation experiments were performed with pulsed laser (Photonics Instruments) tuned to 435nm. Vertices of the cut edges were tracked; the distance of vertex position shifts was measured using Fiji (http://fiji.sc/).

Image processing and automated image analysis

Images were processed and automatically analyzed using custom code in Matlab (KoreTechs), previously described in (Biro et al., 2013).

Volume measurements

Surface rendering and volume calculations were performed with Imaris×64 (Bitplane).

Statistical analyses

Statistical analyses were performed using Matlab software. Mann-Whitney U-test was used to compare statistical significance. The experiments were not randomized, and no statistical method was used to predetermine sample size. Reproducibility of all results was confirmed by independent experiments. All experiments were repeated a minimum of three times.

Supplementary Material

Refer to Web version on PubMed Central for supplementary material.

Acknowledgments

We thank J. Bear, B. Goldstein, A. Ewald, and D. Soroldoni for critical reading. This work was funded by an EMBO Long Term Fellowship to J.S., a Research Fellowship from Trinity College, Cambridge and a Bettencourt-Schueller Foundation Young Researcher Prize to E.H., a Cancer Institute NSW Early Career Researcher fellowship (13/ECF/1-25) and a Cancer Australia/Cure Cancer Australia Foundation project grant (1070498) to M.B., and grants from the NHLBI (HL117164) and NIGMS (GM074104) to J.B.W. JBW was an early career scientist of the Howard Hughes Medical Inst. This work was initiated at the New Quantitative Approaches to Morphogenesis Workshop at UCSB, which is funded in part by the National Science Foundation (PHY11-25915) and the NIGMS (GM067110-05).

References

Biro M, Romeo Y, Kroschwald S, Bovellan M, Boden A, Tcherkezian J, Roux PP, Charras G, Paluch EK. Cell cortex composition and homeostasis resolved by integrating proteomics and quantitative imaging. Cytoskeleton (Hoboken). 2013; 70:741–754. [PubMed: 24136886]

Block J, Breitsprecher D, Kuhn S, Winterhoff M, Kage F, Geffers R, Duwe P, Rohn JL, Baum B, Brakebusch C, et al. FMNL2 drives actin-based protrusion and migration downstream of Cdc42. Curr Biol. 2012; 22:1005–1012. [PubMed: 22608513]

Brooks ER, Wallingford JB. Multiciliated cells. Curr Biol. 2014; 24:R973–R982. [PubMed: 25291643]

Bryant DM, Datta A, Rodriguez-Fraticelli AE, Peranen J, Martin-Belmonte F, Mostov KE. A molecular network for de novo generation of the apical surface and lumen. Nat Cell Biol. 2010; 12:1035–1045. [PubMed: 20890297]

Chung MI, Kwon T, Tu F, Brooks ER, Gupta R, Meyer M, Baker JC, Marcotte EM, Wallingford JB. Coordinated genomic control of ciliogenesis and cell movement by RFX2. Elife. 2014; 3:e01439. [PubMed: 24424412]

Collinet C, Rauzi M, Lenne PF, Lecuit T. Local and tissue-scale forces drive oriented junction growth during tissue extension. Nat Cell Biol. 2015; 17:1247–1258. [PubMed: 26389664]

Cotsarelis G, Cheng SZ, Dong G, Sun TT, Lavker RM. Existence of slow-cycling limbal epithelial basal cells that can be preferentially stimulated to proliferate: implications on epithelial stem cells. Cell. 1989; 57:201–209. [PubMed: 2702690]

Datta A, Bryant DM, Mostov KE. Molecular regulation of lumen morphogenesis. Curr Biol. 2011; 21:R126–R136. [PubMed: 21300279]

Demoulin D, Carlier MF, Bibette J, Baudry J. Power transduction of actin filaments ratcheting in vitro against a load. Proc Natl Acad Sci U S A. 2014; 111:17845–17850. [PubMed: 25453075]

Driessens G, Beck B, Caauwe A, Simons BD, Blanpain C. Defining the mode of tumour growth by clonal analysis. Nature. 2012; 488:527–530. [PubMed: 22854777]

Eisenhoffer GT, Loftus PD, Yoshigi M, Otsuna H, Chien CB, Morcos PA, Rosenblatt J. Crowding induces live cell extrusion to maintain homeostatic cell numbers in epithelia. Nature. 2012; 484:546–549. [PubMed: 22504183]

Evans MJ, Moller PC. Biology of airway basal cells. Exp Lung Res. 1991; 17:513–531. [PubMed: 1860451]

Evans MJ, Van Winkle LS, Fanucchi MV, Plopper CG. Cellular and molecular characteristics of basal cells in airway epithelium. Exp Lung Res. 2001; 27:401–415. [PubMed: 11480582]

Ford JR, Terzaghi-Howe M. Basal cells are the progenitors of primary tracheal epithelial cell cultures. Exp Cell Res. 1992; 198:69–77. [PubMed: 1727059]

Gibson MC, Perrimon N. Extrusion and death of DPP/BMP-compromised epithelial cells in the developing Drosophila wing. Science. 2005; 307:1785–1789. [PubMed: 15774762]

Guillot C, Lecuit T. Mechanics of epithelial tissue homeostasis and morphogenesis. Science. 2013; 340:1185–1189. [PubMed: 23744939]

Gutzman JH, Graeden EG, Lowery LA, Holley HS, Sive H. Formation of the zebrafish midbrain-hindbrain boundary constriction requires laminin-dependent basal constriction. Mech Dev. 2008; 125:974–983. [PubMed: 18682291]

Hannezo E, Prost J, Joanny JF. Theory of epithelial sheet morphology in three dimensions. Proc Natl Acad Sci U S A. 2014; 111:27–32. [PubMed: 24367079]

Heisenberg CP, Bellaiche Y. Forces in tissue morphogenesis and patterning. Cell. 2013; 153:948–962. [PubMed: 23706734]

Kim K, Lake BB, Haremaki T, Weinstein DC, Sokol SY. Rab11 regulates planar polarity and migratory behavior of multiciliated cells in Xenopus embryonic epidermis. Dev Dyn. 2012; 241:1385–1395. [PubMed: 22778024]

Kobielak A, Pasolli HA, Fuchs E. Mammalian formin-1 participates in adherens junctions and polymerization of linear actin cables. Nat Cell Biol. 2004; 6:21–30. [PubMed: 14647292]

Kovar DR, Pollard TD. Insertional assembly of actin filament barbed ends in 18 association with formins produces piconewton forces. Proc Natl Acad Sci U S A. 2004; 101:14725–14730. [PubMed: 15377785]

Lee CJ, EK K, Gray RS, Park TJ, Wallingford JB. Whole-Mount Fluorescence Immunocytochemistry on Xenopus Embryos. Cold Spring Harbor Protocols. 2008

Leung CT, Coulombe PA, Reed RR. Contribution of olfactory neural stem cells to tissue maintenance and regeneration. Nat Neurosci. 2007; 10:720–726. [PubMed: 17468753]

Lu P, Barad M, Vize PD. Xenopus p63 expression in early ectoderm and neurectoderm. Mech Dev. 2001; 102:275–278. [PubMed: 11287210]

Macara IG, Guyer R, Richardson G, Huo Y, Ahmed SM. Epithelial homeostasis. Curr Biol. 2014; 24:R815–R825. [PubMed: 25202877]

Maitre JL, Berthoumieux H, Krens SF, Salbreux G, Julicher F, Paluch E, Heisenberg CP. Adhesion functions in cell sorting by mechanically coupling the cortices of adhering cells. Science. 2012; 338:253–256. [PubMed: 22923438]

Mao Y, Baum B. Tug of war-The influence of opposing physical forces on epithelial cell morphology. Dev Biol. 2015; 401:92–102. [PubMed: 25576028]

Marinari E, Mehonic A, Curran S, Gale J, Duke T, Baum B. Live-cell delamination counterbalances epithelial growth to limit tissue overcrowding. Nature. 2012; 484:542–545. [PubMed: 22504180]

Martin AC, Goldstein B. Apical constriction: themes and variations on a cellular mechanism driving morphogenesis. Development. 2014; 141:1987–1998. [PubMed: 24803648]

Massarwa R, Schejter ED, Shilo BZ. Apical secretion in epithelial tubes of the Drosophila embryo is directed by the Formin-family protein Diaphanous. Dev Cell. 2009; 16:877–888. [PubMed: 19531358]

Mogilner A, Oster G. Force generation by actin polymerization II: the elastic ratchet and tethered filaments. Biophys J. 2003; 84:1591–1605. [PubMed: 12609863]

Moody SA. Fates of the blastomeres of the 16-cell stage Xenopus embryo. Dev Biol. 1987; 119:560–578. [PubMed: 3803718]

Ng MR, Besser A, Brugge JS, Danuser G. Mapping the dynamics of force transduction at cell-cell junctions of epithelial clusters. Elife. 2014; 3:e03282. [PubMed: 25479385]

Pan J, You Y, Huang T, Brody SL. RhoA-mediated apical actin enrichment is required for ciliogenesis and promoted by Foxj1. J Cell Sci. 2007; 120:1868–1876. [PubMed: 17488776]

Prass M, Jacobson K, Mogilner A, Radmacher M. Direct measurement of the lamellipodial protrusive force in a migrating cell. J Cell Biol. 2006; 174:767–772. [PubMed: 16966418]

Rauzi M, Lenne PF, Lecuit T. Planar polarized actomyosin contractile flows control epithelial junction remodelling. Nature. 2010; 468:1110–1114. [PubMed: 21068726]

Rizvi SA, Neidt EM, Cui J, Feiger Z, Skau CT, Gardel ML, Kozmin SA, Kovar DR. Identification and characterization of a small molecule inhibitor of formin-mediated actin assembly. Chem Biol. 2009; 16:1158–1168. [PubMed: 19942139]

Rock JR, Onaitis MW, Rawlins EL, Lu Y, Clark CP, Xue Y, Randell SH, Hogan BL. Basal cells as stem cells of the mouse trachea and human airway epithelium. Proc Natl Acad Sci U S A. 2009; 106:12771–12775. [PubMed: 19625615]

Rosenblatt J, Raff MC, Cramer LP. An epithelial cell destined for apoptosis signals its neighbors to extrude it by an actin- and myosin-dependent mechanism. Curr Biol. 2001; 11:1847–1857. [PubMed: 11728307]

Saotome I, Curto M, McClatchey AI. Ezrin is essential for epithelial organization and villus morphogenesis in the developing intestine. Dev Cell. 2004; 6:855–864. [PubMed: 15177033]

Shen J, Dahmann C. Extrusion of cells with inappropriate Dpp signaling from Drosophila wing disc epithelia. Science. 2005; 307:1789–1790. [PubMed: 15774763]

Sherrard K, Robin F, Lemaire P, Munro E. Sequential activation of apical and basolateral contractility drives ascidian endoderm invagination. Curr Biol. 2010; 20:1499–1510. [PubMed: 20691592]

Sirour C, Hidalgo M, Bello V, Buisson N, Darribere T, Moreau N. Dystroglycan is involved in skin morphogenesis downstream of the Notch signaling pathway. Mol Biol Cell. 2011; 22:2957–2969. [PubMed: 21680717]

Stubbs JL, Davidson L, Keller R, Kintner C. Radial intercalation of ciliated cells during Xenopus skin development. Development. 2006; 133:2507–2515. [PubMed: 16728476]

Szymaniak AD, Mahoney JE, Cardoso WV, Varelas X. Crumbs3-Mediated Polarity Directs Airway Epithelial Cell Fate through the Hippo Pathway Effector Yap. Dev Cell. 2015; 34:283–296. [PubMed: 26235047]

Tsujimura A, Koikawa Y, Salm S, Takao T, Coetzee S, Moscatelli D, Shapiro E, Lepor H, Sun TT, Wilson EL. Proximal location of mouse prostate epithelial stem cells: a model of prostatic homeostasis. J Cell Biol. 2002; 157:1257–1265. [PubMed: 12082083]

Wakatsuki T, Wysolmerski RB, Elson EL. Mechanics of cell spreading: role of myosin II. J Cell Sci. 2003; 116:1617–1625. [PubMed: 12640045]

Werner ME, Hwang P, Huisman F, Taborek P, Yu CC, Mitchell BJ. Actin and microtubules drive differential aspects of planar cell polarity in multiciliated cells. J Cell Biol. 2011; 195:19–26. [PubMed: 21949415]

Werner ME, Mitchell BJ. Understanding ciliated epithelia: The power of Xenopus. Genesis. 2011

Werner ME, Mitchell JW, Putzbach W, Bacon E, Kim SK, Mitchell BJ. Radial intercalation is regulated by the Par complex and the microtubule-stabilizing protein CLAMP/Spef1. J Cell Biol. 2014; 206:367–376. [PubMed: 25070955]

Wu SK, Gomez GA, Michael M, Verma S, Cox HL, Lefevre JG, Parton RG, Hamilton NA, Neufeld Z, Yap AS. Cortical F-actin stabilization generates apical-lateral patterns of junctional contractility that integrate cells into epithelia. Nat Cell Biol. 2014; 16:167–178. [PubMed: 24413434]

Yang C, Czech L, Gerboth S, Kojima S, Scita G, Svitkina T. Novel roles of formin mDia2 in lamellipodia and filopodia formation in motile cells. PLoS Biol. 2007; 5:e317. [PubMed: 18044991]

Yu W, Datta A, Leroy P, O'Brien LE, Mak G, Jou TS, Matlin KS, Mostov KE, Zegers MM. Beta1-integrin orients epithelial polarity via Rac1 and laminin. Mol Biol Cell. 2005; 16:433–445. [PubMed: 15574881]

Highlights

- MPF activation in immature *Xenopus* oocytes requires the ligase activity of APC/C^{Cdh1}
- The catalytic subunit of protein phosphatase PP6 is the relevant APC/C^{Cdh1} substrate
- PP6c destruction enables Aurora-A activation resulting in synthesis of M-phase proteins

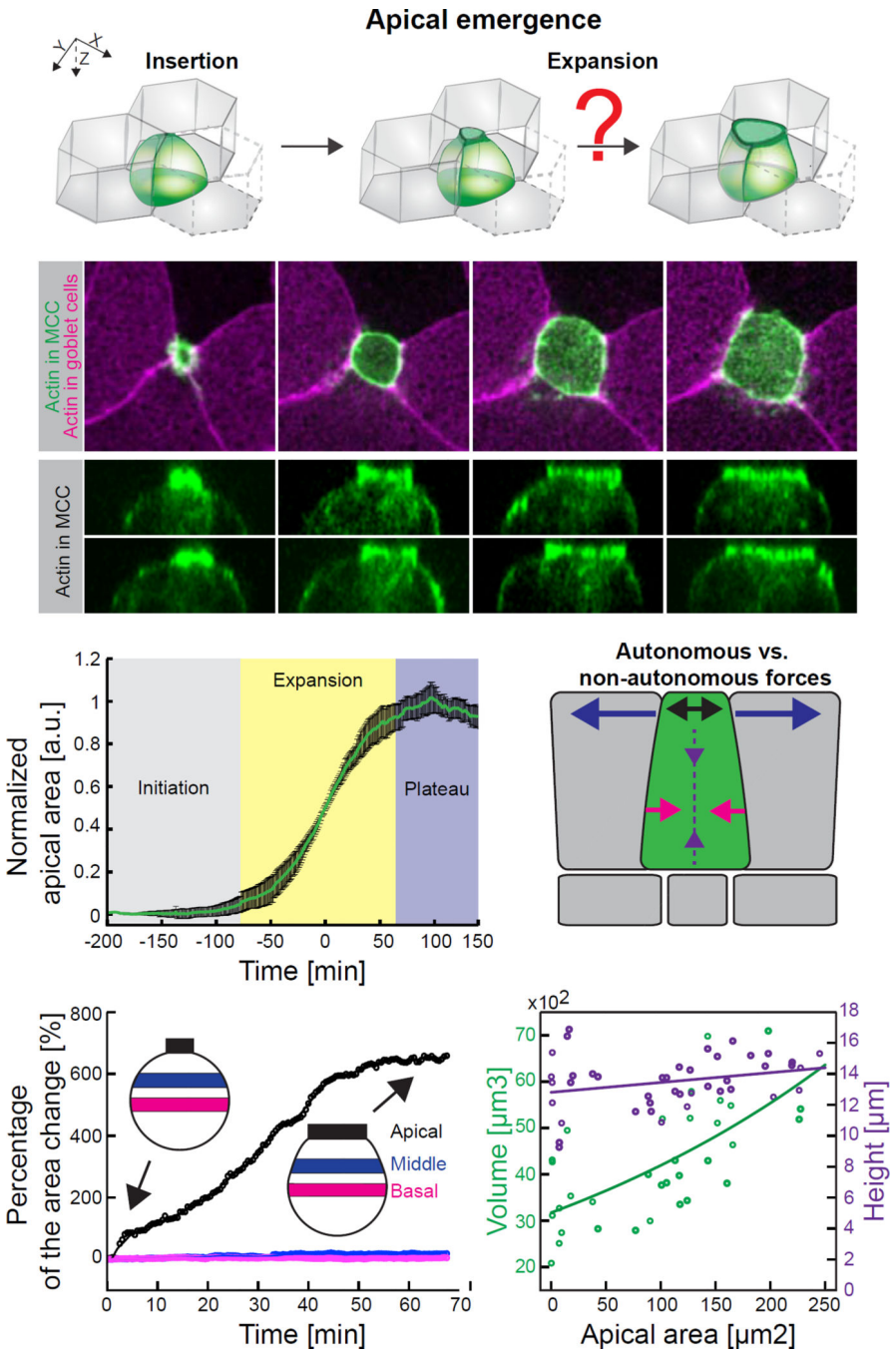

Figure 1. Apical emergence is selectively driven in the apical region of nascent multiciliated cells (MCCs)

(**A**) Schematic of the apical emergence process. Upon insertion at the tricellular junction, a MCC precursor (green) expands its apical surface within the surrounding goblet cells (grey). (**B**) Image sequence of apically emerging MCC expressing actin marker – utrophin (UtrCH, green) under MCC specific α-tubulin promoter; goblet cells visualized by expression of UtrCH-RFP (magenta) under goblet specific nectin promoter. (**C**) Orthogonal projections, corresponding to (B), of apically emerging MCC (visualized by α-tubulin UtrCH-GFP. (**D**)

Three phases of apical area expansion process. Data represent mean (green line) and variance (black bars), n = 9 cells from 9 embryos. (**E**) Schematic of potential autonomous forces (baso-lateral constriction, red arrows; apico-basal squeezing, purple arrows; apical pushing, black arrows) and non-autonomous forces (neighboring pulling, blue arrows) that might contribute to apical expansion process. (**F**) Representative surface area dynamics of the apical (black), middle (blue) and basal (red) region of MCC during apical emergence. Percentage of surface area change is calculated as a ratio of the surface area at the consecutive time point to the surface area at the beginning of the emergence process. Inserts – schematic of MCC at the beginning and at the end of the apical emergence process; average percentage changes of surface areas at given region and SD are: Apical side 618.5 ± 28.03%, Middle side 23.99 ± 28.95%, Basal side 3.24 ± 5.15%, n=5 cells from 5 embryos. (**G**) Volume (green) and height (purple) changes of MCCs throughout apical emergence process. Scale bar, 10μm. a.u., arbitrary units. See also Figure S1 and Figure S2.

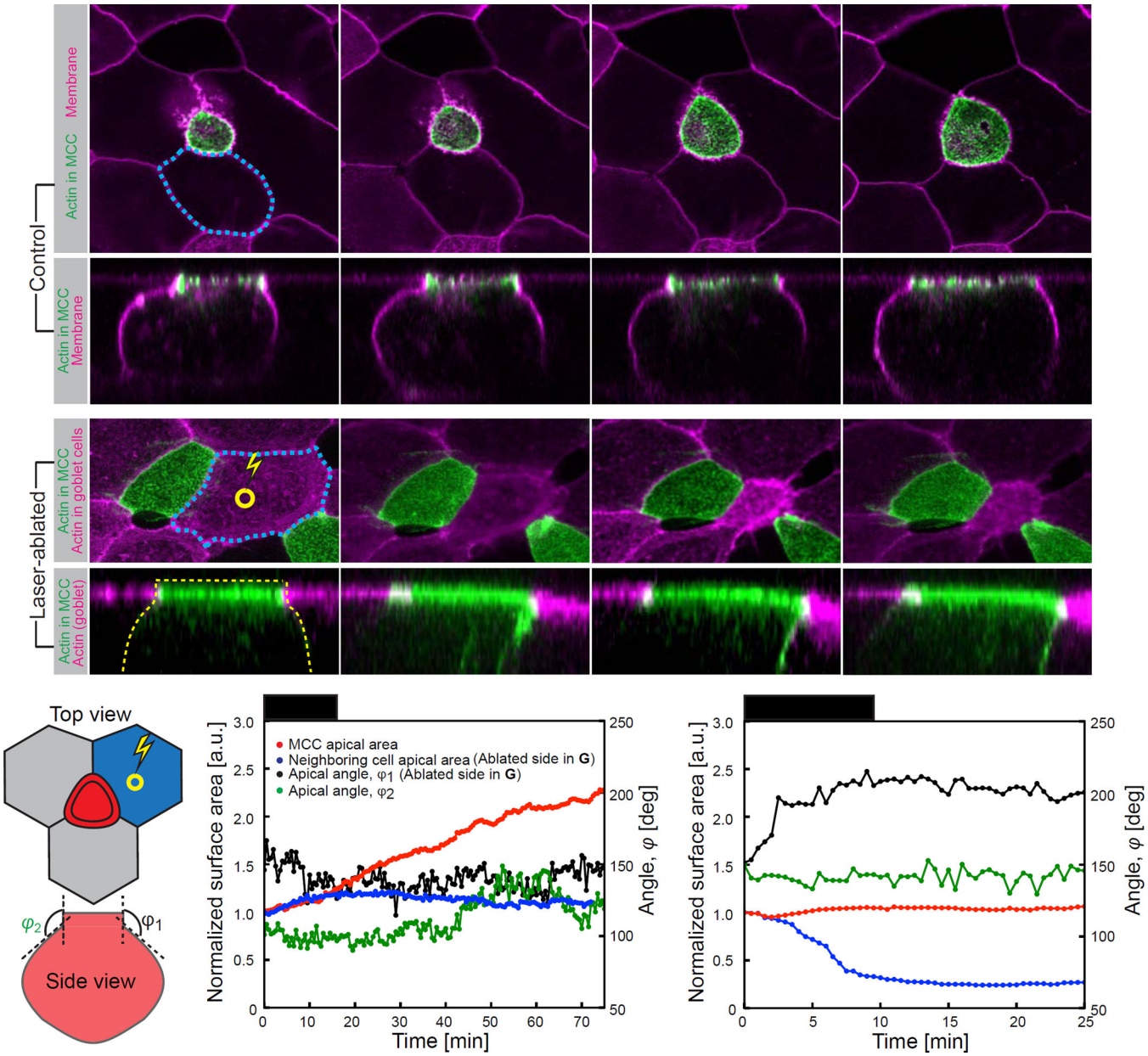

Figure 2. Puling forces of cells adjacent to MCCs do not drive apical emergence process

(A) Image sequence of apically expanding MCC expressing actin marker – utrophin (UtrCH, green) under MCC specific α-tubulin promoter; epithelial cells visualized by expression of membrane marker CAAX-RFP mRNA (magenta). (**B**) Orthogonal projections, corresponding to (A). (**C**) Image sequence of MCC apical domain upon laser ablation in the center (indicated by yellow circle) of the neighboring goblet cell. Laser ablation leads to excessive constriction of goblet cell (outlined in blue dotted line) but does not result in MCC apical domain collapse. (**D**) Orthogonal projections, corresponding to (C). Constricting goblet cell exerts pulling force on the MCC apical domain, as assessed by change of the angle between apical and lateral side of MCC. (**E**) Parameters measured upon laser ablation of goblet cell adjacent to MCC: apical area of ablated goblet cell, blue; apical area of MCC

adjacent to ablated goblet cell, red; angles between apical and lateral side, ϕ_1 (ablated side) and ϕ_2 (non-ablated-side). (**F**) Dynamics of parameters described in (E) in control and upon laser ablation in the center of the goblet cell (**G**). Despite the evident pulling by the neighboring goblet cell (increase of ϕ_1 in (G)), apical area of MCC does not increase, compare to (F). Scale bar, 10μm., a.u., arbitrary units. See also Figure S3.

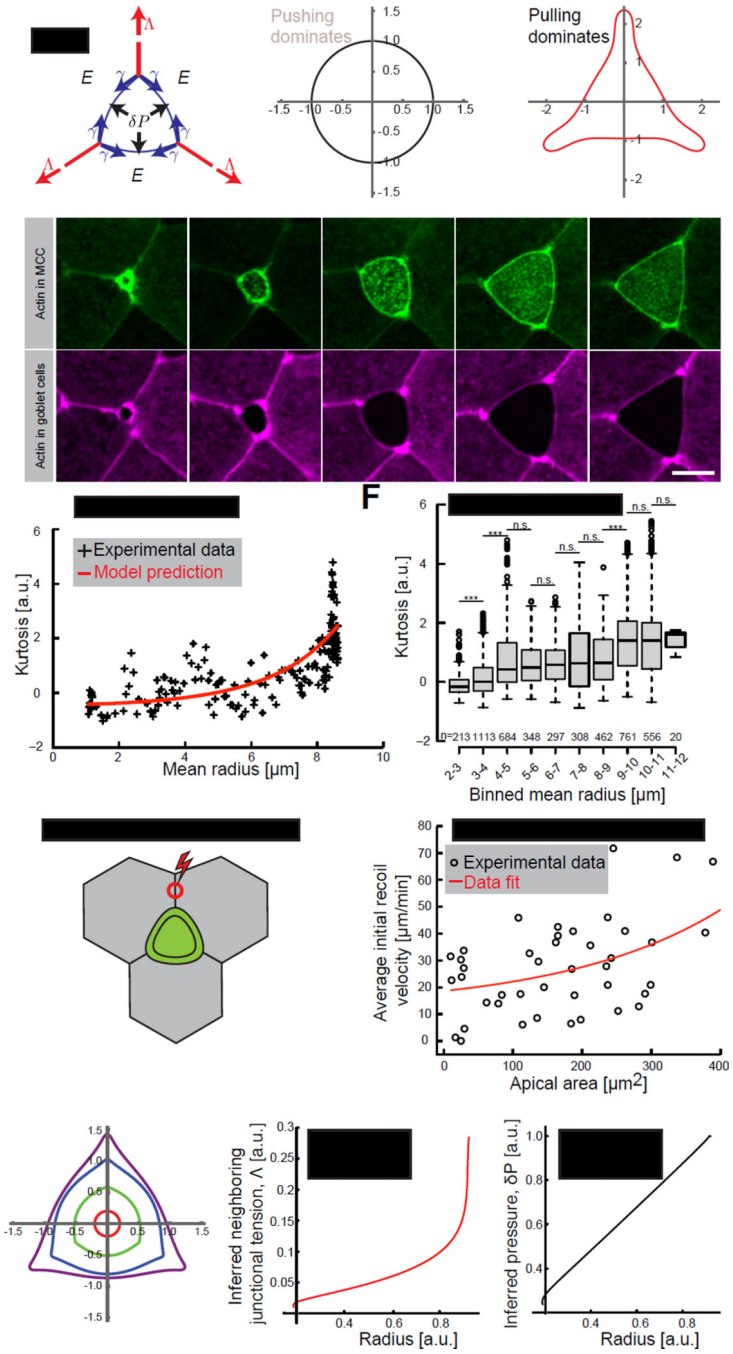

Figure 3. MCC-generated pushing forces majorly drive apical expansion process

(**A**) Schematic of the theoretical model of forces acting on an apical domain of a MCC. Apical domain expanding forces: effective 2D pressure, δP (black arrows) and neighboring junctional pulling forces, Λ (red arrows) acting against MCC cortical tension, γ (blue arrows) and elasticity from the surrounding cells, *E*. (**B**) Simulation of the MCC apical domain shape upon dominant pushing forces or (**C**) dominant junctional pulling forces. (**D**) Image sequence of an apically expanding MCC (visualized by α-tubulin UtrCH-GFP, green) within goblet cells (visualized by nectin UtrCH-RFP, magenta). (**E**) Experimental (black)

and theoretical (red) curvature changes, defined by kurtosis, in time of the cell showed in (D). (**F**) Kurtosis values for the consecutive apical domain sizes, categorized by binned mean radius, in control cells. Boxes extend from the 25^{th} to 75^{th} percentiles, with a line at the median. P values, Mann–Whitney U test (number of embryos, n>5), ***p<0.001, n.s. – not significant. (**G**) Schematic of laser ablation of junctions perpendicular to MCC, red circle represents the ablation region (**H**) Initial recoil velocities upon laser ablation of junctions described in (G). Black circles – experimental data, solid red line – fit. (**I**) Shape simulation of the MCC apical domain based on the theoretical model. (**J**) Inferred neighboring junctional tension, Λ and pressure, δP (**K**) from the simulated shape showed in (D). Scale bar, 10μm. a.u., arbitrary units. See also Figure S4.

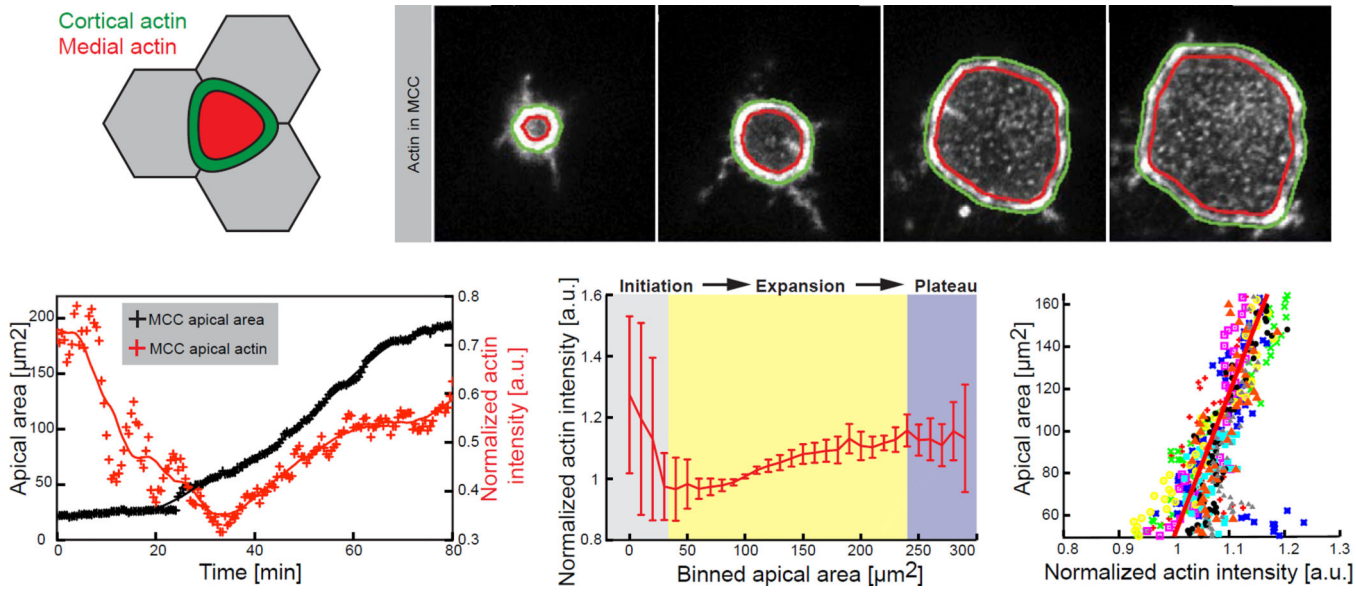

Figure 4. Formation of medial apical actin of MCCs highly correlates with expansion dynamics of the apical domain

(**A**) Segmentation schematic of the cortical (green) and the medial (red) region of a MCC within the plane of the exposed apical area. (**B**) Representative image sequence of automatically segmented cortical and medial region within apically expanding MCC (visualized by α-tubulin UtrCH-GFP). (**C**) Representative - effective actin (ratio of mean medial to mean cortical actin) dynamics (red) during the apical area (black) expansion process. Crosses, data points; line, data smoothed by factor 5. (**D**) Effective apical actin concentration for the consecutive apical domain sizes, categorized by binned area, in control cells, n=9 cells from 9 embryos. Data represent mean and variance. (**E**) Effective apical actin concentration as a function of apical area in control cells, n=9 cells from 9 embryos. Scale bar, 10µm. a.u., arbitrary units.

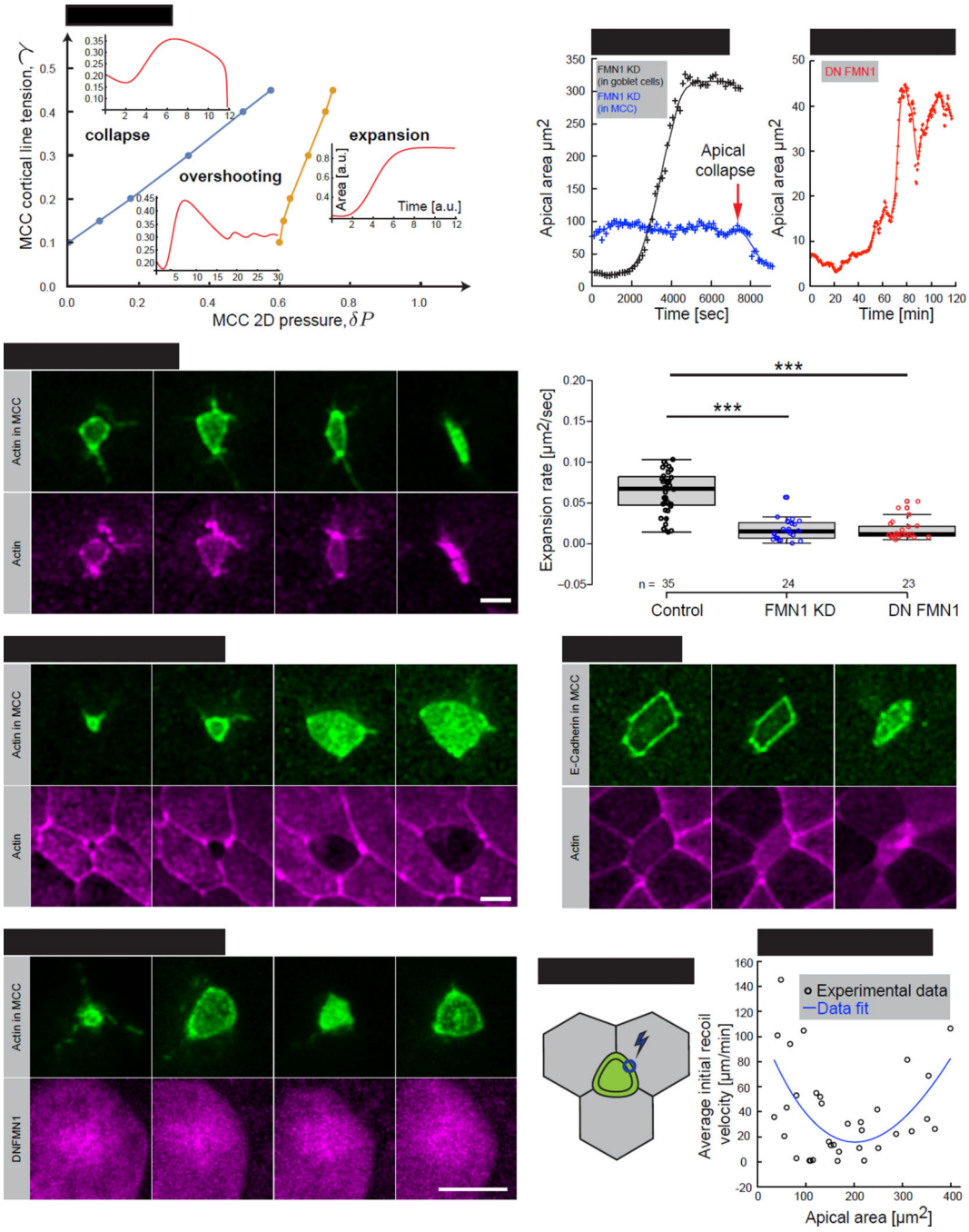

Fig.5. Actin polymerization and subsequent actin network formation drive apical expansion of MCCs

(**A**) Phase diagram of possible apical domain expansion dynamics, as a function of target MCC cortical tension γ and pressure δP. A blue and an orange line indicate the transition zones between different phases. Inserts represent simulations of the apical area in time for the three regimes. (**B**) Image sequence of apically collapsing MCC (4 out of 4 cells), (visualized by α-tubulin UtrCH-GFP, green) upon mosaic co-injection of FMN1 morpholino (FMN1 MO) with UtrCH-RFP mRNA, magenta). Note that FMN1 MO is present only in

MCC, as indicated by UtrCH-RFP mRNA expression (**C**) Image sequence of apically expanding MCC (visualized by α-tubulin UtrCH-GFP, green) upon mosaic co-injection of FMN1 morpholino (FMN1 MO) with UtrCH-RFP mRNA, magenta). Note that FMN1 MO is present only in goblet cells and that MCC expands normally (4 out of 4 cells). (**D**) Image sequence of MCC (visualized by α-tubulin UtrCH-GFP, green) expressing dominant negative FMN1 (DNFMN1, visualized by α-tubulin DNFMN1-RFP, magenta). (**E**) Apical area dynamics of MCC upon mosaic injection of FMN1 MO (black – FMN1 MO present in MCCs only (showed in (B)), blue – FMN1 MO present in goblet cells only (showed in (C)). (**F**) Apical area dynamics of MCC expressing dominant negative FMN1 (DN FMN1), representing an "overshooting" regime within the phase diagram. (**G**) Apical expansion rate during linear growth phase in controls (black), MCCs FMN1 KD (blue), and MCCs expressing dominant negative FMN1 (DN FMN1), number of embryos, n>15. Boxes extend from the 25^{th} to 75^{th} percentiles, with a line at the median. P values calculated with Mann–Whitney U test, ***p<0.001 (**H**) Image sequence of apically collapsing MCC (visualized by α-tubulin E-Cadherin-GFP, green) within goblet cells (visualized by nectin RFP-UtrCH, magenta) upon treatment with 50μm of SMIFH2. Time indicates minutes after drug addition to the medium. (**I**) Laser ablation schematics of MCC junctions, blue circle represents the ablation region. (**J**) Initial recoil velocities upon laser ablation of MCCs junctions described in (J). Black circles – experimental data, solid blue line – fit. Scale bar, 10μm. a.u., arbitrary units. See also Figure S5.

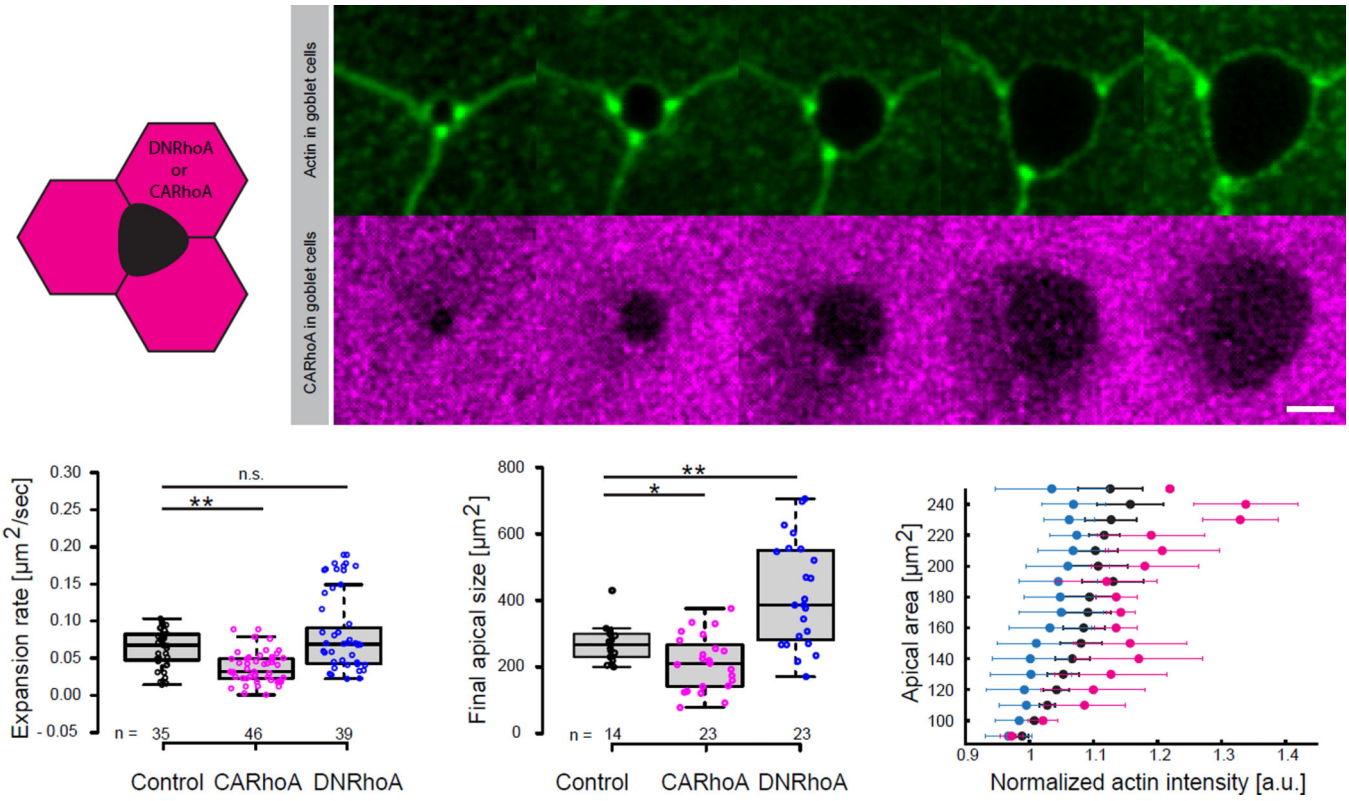

Figure 6. Apical emergence of MCCs is influenced by external rigidity of the surrounding cells

(A) Schematic of nectin driven expression (goblet cells specific) of DNRhoA or CARhoA. (**B**) Image sequence of apically expanding MCC, outlined by expression of UtrCH-GFP under nectin promoter (top, green), within goblet cells expressing CARhoA under nectin promoter (bottom, magenta). (**C**) Apical expansion rate during linear growth phase in controls (black), MCCs surrounded by goblet cells expressing -CARhoA (magenta), -DNRhoA (blue), **p<0.01, n.s. – not significant. (**D**) Final size of the apical domain of MCCs for experimental conditions described in C, **p<0.01, *p<0.05 (**E**) Effective apical actin concentration in MCCs as a function of apical area in controls (black crosses), MCC surrounded by goblet cells expressing: CARhoA (magenta), DNRhoA (blue); data represent mean and variance (number of embryos, n>5). Boxes extend from the 25th to 75th percentiles, with a line at the median. P values, Mann–Whitney U test (number of embryos, n>5), n.s., not significant. Scale bar, 10µm. a.u., arbitrary units.